Two-dimensional carbon nitride C_6N nanosheet with egg-comb-like structure and electronic properties of a semimetal

Two-dimensional carbon nitride C_6N nanosheet with egg-comb-like structure and electronic properties of a semimetal

A. Bafekry[1,2,*] M. Shahrokhi[3], A. Shafique[4], H. R. Jappor[5], F. Shojaei[6], S. A. H. Feghhi[2], M. Ghergherehchi[8], and D. Gogova[9]

[1] *Department of Physics, University of Antwerp, Groenenborgerlaan 171, B-2020 Antwerp, Belgium*
[2] *Department of Radiation Application, Shahid Beheshti University, Tehran, Iran*
[3] *Department of Physics, Faculty of Science, University of Kurdistan, 66177-15175 Sanandaj, Iran*
[4] *Department of Physics, Lahore University of Management Sciences,Lahore, Pakistan*
[5] *Department of Physics, College of Education for Pure Sciences, University of Babylon, Hilla, Iraq*
[6] *Department of Chemistry, Faculty of Sciences, Persian Gulf University, Bushehr 75169, Iran*
[7] *Department of Physics, University of Oslo, P.O. Box 1048, Blindern, Oslo, Norway*
[8] *College of Electronic and Electrical Engineering, Sungkyun Kwan University, Suwon, Korea*

(Dated: December 22, 2020)

In this study, the structural, electronic and optical properties of theoretically predicted C_6N monolayer structure are investigated by means of Density Functional Theory-based First-Principles Calculations. Phonon band dispersion calculations and molecular dynamics simulations reveal the dynamical and thermal stability of the C_6N single-layer structure. We found out that the C_6N monolayer has large negative in-plane Poisson's ratios along both X and Y direction and the both values are almost four times that of the famous-pentagraphene. The electronic structure shows that C_6N monolayer is a semi-metal and has a Dirac-point in the BZ. The optical analysis using the RPA method constructed over HSE06 illustrates that the first peak of absorption coefficient of the C_6N monolayer along all polarizations is located in the IR range of spectrum, while the second absorption peak occurs in the visible range, which suggests its potential applications in optical and electronic devices. Interestingly, optically anisotropic character of this system is highly desirable for the design of polarization-sensitive photodetectors. Thermoelectric properties such as Seebeck coefficient, electrical conductivity, electronic thermal conductivity and power factor are investigated as a function of carrier doping at temperatures 300 K, 400 K, and 500 K. In general, we predict that the C_6N monolayer could be a new platform for study of novel physical properties in two-dimensional semi-metal materials, which may provide new opportunities to realize high-speed low-dissipation devices.

I. INTRODUCTION

The discovery of the first atomically thin two-dimensional (2D) material-Graphene [1]- with magnificent properties, which have never been observed before, has triggered tremendous pure scientific and technological interest. A huge number of researchers has devoted enormous efforts in exploration of the monolayer carbon and in development of novel 2D materials beyond Graphene. To illustrate, the most noticeable properties are ambipolar electric field-effect [2], large surface area, the top-notch flexibility [3, 4], ascending thermal (5×10^3 W/mk) [5] and electrical conductivity [6], marvelously fracture strength (130 GPa) [2, 7, 8], very high optical transmittance (97.7%) [9], excellent electron mobility (2×10^5 $cm^2v^{-1}s^{-1}$) [10, 11], ultrahigh Young's modulus (1.1 TPa) [12], and the exotic quantum Hall effect at room temperature [13, 14]. Notwithstanding these idealistic properties, there are two drawbacks restricting its applications: (i) mechanical instability - the propency to collaps and to form crispiness and (ii) electrical - the zero energy band-gap. [15, 16]. Complementary to this, materials with comparatively poor carrier mobility cannot be employed in the applications used in the high-performance electronics [17, 18]. These obstacles encouraged researchers, to devote their research efforts to development of 2D materials with unique properties; by peeling of bulk materials or chemical vapor deposition [19, 20]. Indeed, many researchers have been undertaken to look for ways to open the energy gap of graphene by defects [21, 22], strain [23–27], and doping [28]. Another group of researchers have tried to find alternative 2D materials beyond graphene. Nowadays, a new technology has emerged and a considerable amount of technological work has been made to develop and manufacture 2D carbon-based semiconductor materials. Strictly speaking, by making a 2D lattice crafted of certain ratios of nitrogen (N) and carbon (C) elements. However, in addition to being a neighbor to C in the periodic table, N tends to be an appropriate companion and partner, to build another significant collection of 2D materials, known as carbon nitride monolayers.

To date, researchers have explored many kinds of carbon nitride nanosheets encompassing CN [29], CN_2 [30],C_2N [31, 32], C_3N, C_4N_3 [33–35], triazine C_3N_3 [36], C_3N_5 [37, 38], C_3N_6 [39], C_3N_4 [40, 41], C_7N_6 [42], C_7N_6 [43], C_6N_8 [44, 45], C_6N_6 [46, 47], C_9N_4 [48], and C_2N [49]. Equally important, some of these carbon nitride nanosheets have recently been successfully synthesized, among them are CN, C_2N, C_3N, C_3N_4, C_6N_6, and

C_6N_8 monolayers [50–57]. The aforementioned studies have manifested that 2D carbon nitride allotropes possess disaccorded optical, electronic, thermal, and mechanical properties based on both the strength of the covalent bond and the contribution of carbon and nitrogen atoms (C/N ratios) to the atomic lattice [58–60]. Immensely, the control in the C/N ratio is a useful method to retain the outstanding properties of component materials and lead to other novel physical phenomena. Consequently, carbon nitrides have been extensively proposed as a potential nominee for commonly ongoing applications such as catalysis [61], photocatalyst [62], nanoelectronic devices [60–63], energy storage [64–67], sensors [68, 69], and water splitting [70, 71].

Despite of the large number of papers on carbon nitride allotropes, to the best of our knowledge there is no investigation devoted to the synthesis and study of electronic, optical and thermoelectric properties of a carbon nitride monolayer with a composition formula C_6N. To bridge this gap, we sought in the present work to build a novel carbon nitride 2D material with a C_6N stoichiometry, comprising 10 carbon nitride rings (5 hexagons, 2 pentagons, and 3 tetragons). The remaining part of the paper will calculate the structural, electronic, optical and thermoelectric properties of C_6N carbon nitride monolayer. The pentagons and tetragons rings are designed to significantly change the properties of carbon nitride since the incorporation of these rings produces a positive local Gaussian curvature as reported previously in graphene [72, 73]. Stirringly, it is found that C_6N is a semimetal with one Dirac-point and dynamically more stable relative to other carbon based 2D materials. As a result, our various carbon nitride architectures allow the practical construction of new carbon nitride structures for a wide range of potential applications.

II. METHOD

In this work, we report results of our DFT calculations for the electronic structure as implemented in the OpenMX 3.8 package [76]. The Perdew-Burke-Ernzerhof approach from the generalized gradient approximation (PBE-GGA) [74] is applied to describe the exchange-correlation functional. The norm-conserving pseudopotentials [75] The wave functions are expanded by the linear combination of multiple pseudoatomic orbitals (LCPAOs) generated using a confinement scheme [77, 78]. After the convergence tests, the cutoff energy of 450 eV is chosen so that the total-energy converges below 1.0 meV/atom. The geometries were fully relaxed until the force acting on each atom was less than 1 meV/Å. The k-points for sampling over the Brillouin zone (BZ) integration were generated using the Monkhorst-Pack scheme [79]. The integration over the k-point mesh was performed using $19 \times 19 \times 1$ for the primitive unit cell. The empirical dispersion method of the DFT-D3 [80] is employed to get insight in the van der Waals interactions. Simulated scanning tunneling microscopy (STM) images were obtained using the Tersoff-Hamann theory [81]. STM simulated images and were graphed using WSxM software [82].

Since the C_6N lattice is a low-symmetry lattice, the examination of the dynamical stability with the common DFT approach is computationally demanding. Therefore, in this work the examination of dynamical stability is achieved by using machine-learning interatomic potentials [86–88]. To achieve this aim we have employed the moment tensor potential (MTP) [89], which has been proven as an accurate and computationally efficient model for describing the atomic interactions [90]. We used MLIP package for the calculation of forces using the MTP [91]. The training set is prepared by conducting ab-initio molecular dynamics (AIMD) simulations over $2 \times 2 \times 1$ supercells with $2 \times 2 \times 1$ k-point grids. AIMD simulations are carried out at 50 and 600 K, each for 1000 time steps. Half of the AIMD trajectories are selected to create the training sets. MTP for the C_6N monolayer is then trained passively using the procedure explained in the recent studies [86–88]. The PHONOPY code [92] is employed to obtain phonon dispersion relation over $5 \times 5 \times 1$ supercells using the trained MTP for the force calculations [86, 87].

In the case of optical properties, the real and imaginary parts of dielectric tensor, absorption coefficient and reflectivity were calculated using the random phase approximation (RPA) [83] method constructed over the screened hybrid Heyd-Scuseria-Ernzerhof hybrid functional (HSE06) [84]. Thermoelectric properties are calculated by solving the semi-classical Boltzmann transport equation within the rigid band and constant relaxation time approximations as implemented in the Boltztrap2 code[93]. The values of $\sigma_{\alpha\beta}(\epsilon)$ are directly calculated through the Fourier interpolation of the energy bands. Therefore, a very fine mesh should be required. We have used a k-mesh of $30 \times 30 \times 1$ is employed for calculation of the transport coefficients.

III. STRUCTURAL PROPERTIES

The geometric atomic structure of the C_6N monolayer and its rectangular primitive unit cell is shown in Fig. 1(a). The slightly puckered honeycomb structure of C_6N monolayer exhibits the space group of P_{3m1}. The primitive unit cell is formed by 28 atoms (involving 24 C and 4 N atoms). After structure optimization the lattice constants were demonstrated as: a=7.19 Å and b=8.01 Å. The 3D view of optimized atomic structure of C_6N monolayer with structural parameters such as bond length and bond angles is shown in Fig. 1(b). In the C_6N structure lattice, we can see tree types of rings involving consist

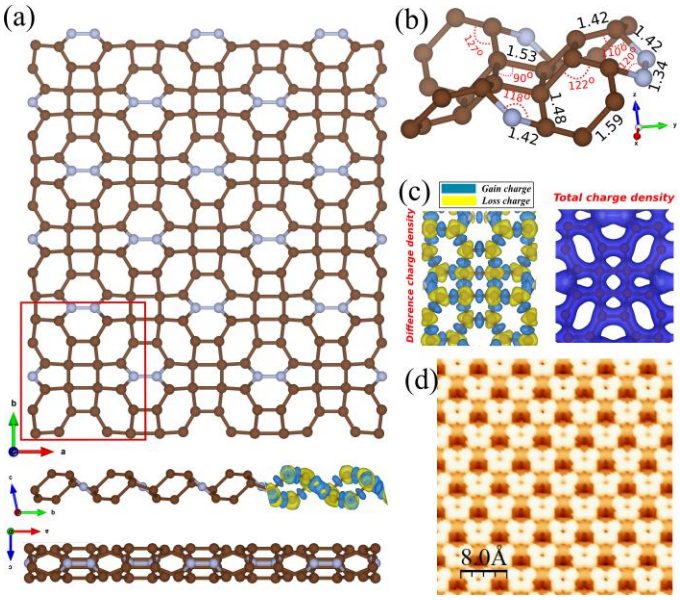

FIG. 1. (a) Geometric atomic structure of C_6N monolayer with its rectangular primitive unit cell indicated by the red square. C and N atoms are represented with brown and blue spheres, respectively. The difference and total charge densities are indicated as inset, the charge accumulation and depletion are shown by color scheme with blue and yellow regions, respectively. (b) 3D view of optimized atomic structure of C_6N monolayer with structural parameters such as bond length and bond angles. (c) The STM simulated image of C_6N monolayer.

of C-C octagon; C-N pentagon; C-C and C-N hexagon. The bond lengths in the C-C octagon ring is determined d_{CC}=1.53 Å and the bond angle θ_1=90°. In the C-N pentagon ring, the d_{CC}=1.48 Å and d_{CN}=1.42 Å as well as the bond angle of C-N-C is 118°. Notice that in the C-C hexagon ring, d_{CC} is determined to be 1.59 Å with a bond angle of 122°. While in the C-N hexagon ring d_{CC}, d_{CN} and d_{NN} are calculated 1.34, 1.42 and 1.42 Å, respectively with a bond angle of the C-N-C is 118°. The optimized structure of the C_6N monolayer is not planar and has a thickness parameter of t=1.71 Å.

The difference and total charge densities are indicated in Fig. 1(c). The charge accumulation and depletion are shown by color schemes with blue and yellow regions,respectively. The difference charge density ($\Delta\rho$) is calculated using the following equation:

$$\Delta\rho = \rho_{tot} - \rho_C - \rho_N \qquad (1)$$

where ρ_{tot}, ρ_C and ρ_N represent the charge densities of the C_6N monolayer and isolated atoms, respectively. The result of difference charge density calculations gives the positively charged C atoms are surrounded by negatively charged N atoms. Based on the charge transfer analysis, we found out that the N atoms gain as $0.31e$ from the adjacent C atoms. According to the Pauling electronegativity scale, the N (3.0) atom has a larger electronegativity than C (2.5) and it results in large difference of electron density. The STM simulated image is obtained from first-principles DFT calculations in order to provide visible guidance for experimental observations (see Fig. 1(d)). The atomistic structure is easily recognized from the predicted STM image, where the N atoms are brighter than the C atoms.

The cohesive energy per atom that is quantifying the stability of materials is calculated using the following equation:

$$E_{coh} = [(n_C E_C + n_N E_N) - E_{tot}]/(n_C + n_N), \qquad (2)$$

where E_C and E_N represent the energies of isolated single C and N atoms; E_{tot} represents the total energy of the C_6N monolayer. In addition, n_C and n_N stand for the number of C and N atoms in the primitive unitcell, respectively. The calculated cohesive energy for the C_6N monolayer is -6.40 eV/atom, which is almost equal or even lower than the corresponding values of other experimentally synthesized carbon nitride monolayers studied in a previous work (β-C_3N_4 (∼-5.85 eV/atom), g-C_3N_4(∼-6.10 eV/atom), g-CN (∼-6.30 eV/atom), and g-C_4N_3(∼-6.40 eV/atom)) [94] indicating its possible experimental synthesis. We have also calculated the formation energy of the C_6N monolayer with respect to the chemical potential of C in perfect graphene and the chemical potential of N in N_2. Similar to other 2D carbon nitride monolayers, the formation energy of C_6N is also positive and its magnitude of 0.18 eV/atom is in the same range as those calculated for the graphitic N-doped graphene with nitrogen concentration of approx. 14% (C_7N and C_5N) [95].

Using density functional theory (DFT), we are able to investigate the stability of C_6N monolayer. The dynamical stability is examined by calculating its phonon band dispersions and is presented in Fig. 2. We first examine the dynamical and thermal stability of C_6N monolayer, by evaluating the phonon dispersion relation and AIMD trajectories at 300 K, respectively. As shown in Fig. 2(a), the phonon dispersion relation is free of any imaginary frequency, confirming the dynamical stability. As the signature of 2D materials, the plotted phonon dispersion relation presents three acoustic modes, two with linear and the other one with a quadratic dispersion. Ab initio molecular dynamics (AIMD) for C_6N monolayer at room temperature is shown in Fig. 2(b). Insets of panel of Fig. 2(b), show the temperature fluctuation and the top-view of the structure after 5 ps of simulation. Analysis of the AIMD trajectories also shows that the structure could stay intact at 300 K, with very stable energy and temperature profiles, proving the thermal stability of the C_6N monolayer.

TABLE I. Structural and electronic parameters of the optimized C_6N monolayer including: lattice constants a and b, average bond length betweens C-C atoms (d_{CC}), C-N atoms (d_{CN}) and N-N atoms (d_{NN})), bond angles between C-C-C atoms (θ_1) and C-N-N (θ_2), thickness defined by the distance between the largest and smallest z coordinates of C atoms (t); cohesive energy per atom, (E_{coh}); charge transfer (ΔQ) between atoms; electronic states (ES) are specified as semimetal (SM).

Sys.	a (Å)	b (Å)	d_{CC} (Å)	d_{CN} (Å)	d_{NN} (Å)	θ_1 (°)	θ_2 (°)	t (Å)	E_{coh} (eV/atom)	ΔQ (e)	ES
C_6N	7.19	8.01	1.34-1.48	1.42	1.42	118	122	1.71	-6.40	0.31	SM

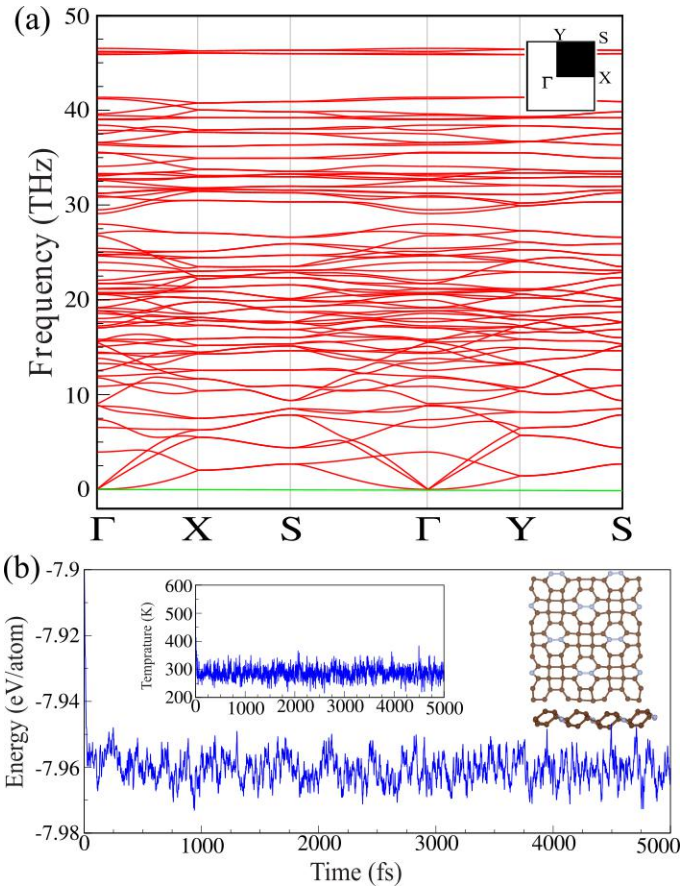

FIG. 2. (a) Phonon band dispersion of C_6N monolayer. (b) Ab initio molecular dynamics (AIMD) for C_6N monolayer at room temperature. Insets of panel show the temperature fluctuation and the top-view of the structure after 5 ps of simulation.

IV. MECHANICAL PROPERTIES

Furthermore, we have evaluated of the mechanical stability of the C_6N monolayer by calculating its linear elastic constants. The strain energy, caused by different types of uniaxial (x and y directions) and biaxial strains, is supposed to be always positive for a carefully relaxed 2DM and it is defined as:

$$E_s = 1/2C_{11}E_1^2 + 1/2C_{22}E_2^2 + C_{12}E_1E_2 + 2C_{66}E_6 \quad (3)$$

where the E_s, E_1, E_2 and E_6 are strain energy per unit area, uniaxial strains along the X and Y axes, and shear strain along the XY direction, respectively. Within the framework of harmonic approximation the C_6N monolayer with a rectangular lattice has three independent elastic constants of C_{11}, C_{22}, C_{12} and C_{66}. The C_6N monolayer is mechanically stable if it satisfies the Born criteria [96] for rectangular lattices: $C_{11}C_{22} - C_{12}^2 > 0$, and $C_{66} > 0$. According to our calculations C_{11}, C_{22}, C_{12} and C_{66} are found to be 191.28, 174.66, -40.77, and 52.87 N/m, respectively. Obviously, these values satisfy the Bron criteria for the rectangular lattice, confirming the mechanical stability of the C_6N monolayer. To further describe the mechanical properties of the C_6N monolayer, we have calculated its in-plane stiffness (C) and Poisson's ratio (ν) along X and Y directions. The in-plane stiffness along X and Y directions are obtained using $C_x = \frac{C_{11}C_{22}-C_{12}^2}{C_{22}}$ and $C_y = \frac{C_{11}C_{22}-C_{12}^2}{C_{11}}$. The calculated C_x and C_y for the C_6N monolayer are 181.77 and 165.98 N/m, respectively. The calculated stiffness values are almost a half of graphene (347 N/m), indicating that the material is appreciably softer than graphene [97]. The Poisson's ratio, which is a dimensionless quantity and describes the expansion or contraction of the material along the perpendicular direction to the direction of applied strain, is obtained using $\nu_x = \frac{C_{12}}{C_{22}}$ and $\nu_y = \frac{C_{12}}{C_{11}}$. The quantity is positive for most of the 2D materials and only a few 2D monolayers are predicted to possess negative Poisson's ratios [98–101]. Interestingly, the C_6N monolayer has negative Poisson's ratios of -0.25 and -0.22 along X and Y directions, respectively, indicating that if the material expands along X or Y direction, it expands instead of contracting along the perpendicular direction. The calculated Poisson's ratios are almost 4 times larger than that obtained for the famous penta-graphene [102].

V. ELECTRONIC PROPERTIES

The results of the electronic structure calculations, i.e., the total density of states (DOS) and the partial DOS (PDOS) of the C_6N monolayer are presented in Fig. 3(a,b). The k-path of BZ is depicted in the inset. The computations show that the C_6N monolayer is a semi-metal, with a zero gap, together with the valence and conduction bands touched and formed a Dirac point

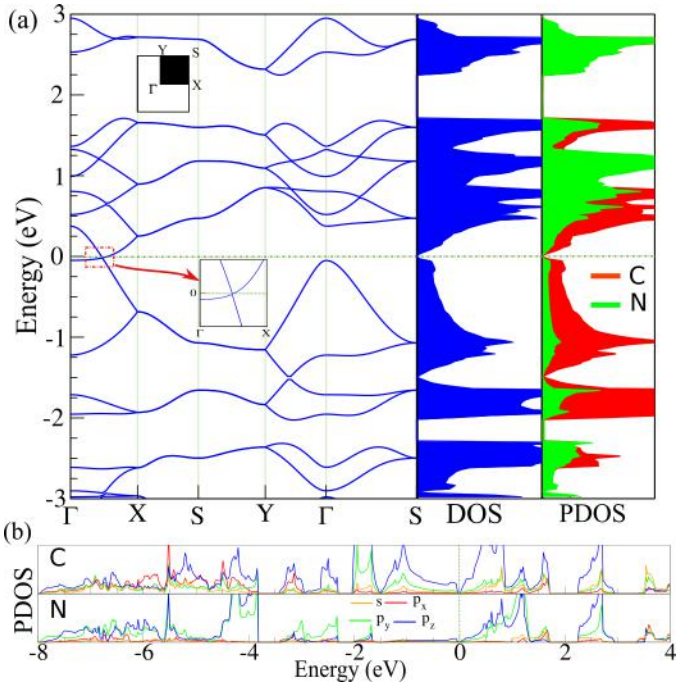

FIG. 3. (a) Electronic band structure, DOS and PDOS of C_6N monolayer. The k-path of BZ is depicted in the inset. Fermi level is set to zero. (b) Calculated PDOS of atoms in C_6N monolayer with respect to p_x, p_y and p_z orbitals.

at between the Γ-X points in the BZ. Notice, the semi-metallic characteristic is preserved when the HSE06 is included. From the DOS and PDOS illustrated in Fig. 3(a), it is clearly seen that the semi-metallic characteristic bands around the Fermi level are mainly composed of C and N atoms does not show any contribution. The orbital-projected DOS diagram of the C_6N monolayer is depicted in Figs. 3(b). The additive of p_x, p_y and p_z orbitals are shown by red, green and blue colors. Blue and red circles illustrate the location of a Dirac cone which is related to the electrons. The Dirac point is composed of the intersection of two bands formed by the p_x, p_y and p_z orbitals centered along the Γ-X point in the Brillouin zone. From Fig. 3(b), we can see that the states energy range between -2.0 and 0.0 eV below the Fermi energy is composed of the C orbital states.

It should be noted that the majority of carbon-nitride monolayers are semiconductors, such as the C_3N_4, C_3N, C_2N, C_7N_6, C_3N_5 and C_3N_6 [39, 50–57]. Recently C_9N_4 was predicted to be a metal, with remarkable states around the Fermi level [43]. This highlights that in comparison with previous theoretically predicted or experimentally fabricated carbon-nitride monolayers, C_6N offers a novel electronic nature of semimetal.

VI. OPTICAL PROPERTIES

The optical responses of this novel 2D system have been considered using the RPA method constructed over HSE06. Because of the asymmetric geometry along the x-, y- and z axes the optical spectra are aisotropic for light polarizations along the in-plane (E‖x and E‖y) and out-of-plane (E‖z) directions. Hence, the optical properties for E‖x, E‖y and E‖z are considered. The imaginary and real parts of the dielectric function (Im(ε) and

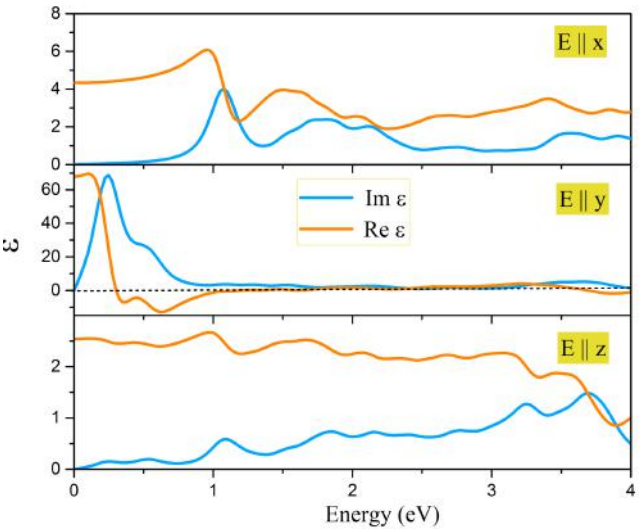

FIG. 4. Imaginary (Im(ε)) and real parts (Re(ε)) of the dielectric function vs. photon energy of the C_6N monolayer, predicted using the RPA + HSE06 approach.

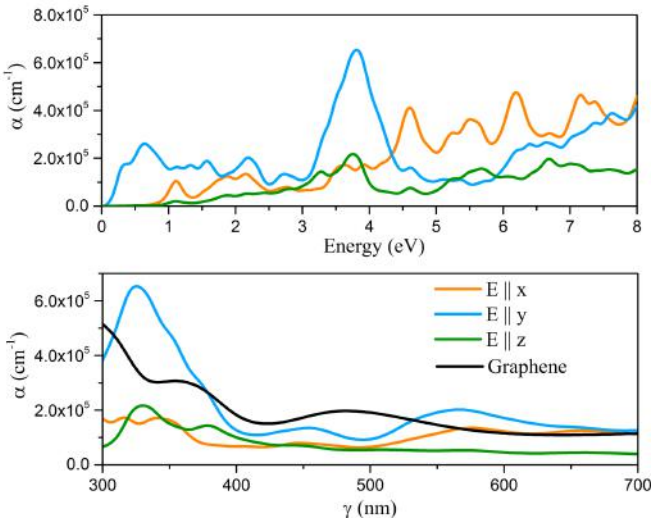

FIG. 5. Optical absorption spectra vs. photon energy (top panel) of the C_6N monolayer, predicted using the RPA + HSE06 approach. Bottom panel shows a comparison of optical absorption spectra as a function of wavelength, for aforementioned nanosheet in the UV-vis range (350-700 nm) of spectrum including graphene (black line).

Re(ε), respectively) of the C_6N monolayer versus photon energy for all polarization directions are illustrated in Fig. 4. It can be seen that the Im(ε) along x- and z-axes starts with a gap which confirms the semiconductor characters of the optical spectra along these directions. The first peak of Im(ε) for the C_6N monolayer occurs at an energy of ∼1.1 and 0.26 eV along the x-axis and z-axis, respectively, which are in IR range of spectrum. Furthermore, the positive values of the static dielectric constant (the values of Re(ε) at zero energy) indicate the semiconductor character of the optical spectra along E‖x and E‖z for this 2D system. The values of the static dielectric constant for the novel 2D carbon nitride system were calculated to be 4.34 and 2.55 along E‖x and E‖z, respectively. In contrast, the Im(ε) along y-axis starts without any gap, presenting weak semiconducting optical responses in this direction. The first peak of Im(ε) occurs at 0.25 eV which is in the IR range. The value of the static dielectric constant along E‖y was estimated to be 68.3. The absorption coefficient of the C_6N monolayer is plotted in Fig. 5. In this case we have also compared the acquired results with that of pristine graphene (black line) in the UV-vis range of light (from 300 to 700 nm) as a function of wavelength from our previous studies [6, 7]. These results indicate that the first absorption peaks for the C_6N monolayer are 1.11, 0.33 and 1.05 eV along x-, y- and z-axes, respectively, which are indeed in the IR range. The second absorption peaks for E‖x and E‖z are located at photon energies greater than 1.5 eV, i.e. in visible range. The results obtained indicate that the C_6N monolayer can enhance UV-vis light absorption in comparison with graphene, which can be potentially attractive for optoelectronic applications. In general, high absorption coefficients were attained (∼10^5 cm^{-1}) for this novel structure which is higher than the typical absorption coefficient value for direct band gap semiconductors across the entire UV-vis range [8]. Interestingly, the optically anisotropic character of this system is highly desirable for the design of polarization-sensitive photodetectors [9].

VII. THERMOELECTRIC PROPERTIES

The C_6N monolayer of shows large intrinsic Seebeck coefficient values for both type of carrier doping (n-type and p-type) in both directions as shown in Fig. 6(a, b). The Seebeck coefficient (S), electrical conductivity ($\sigma^{\alpha\beta}$), and electronic thermal conductivity ($\kappa_e^{\alpha\beta}$) are obtained

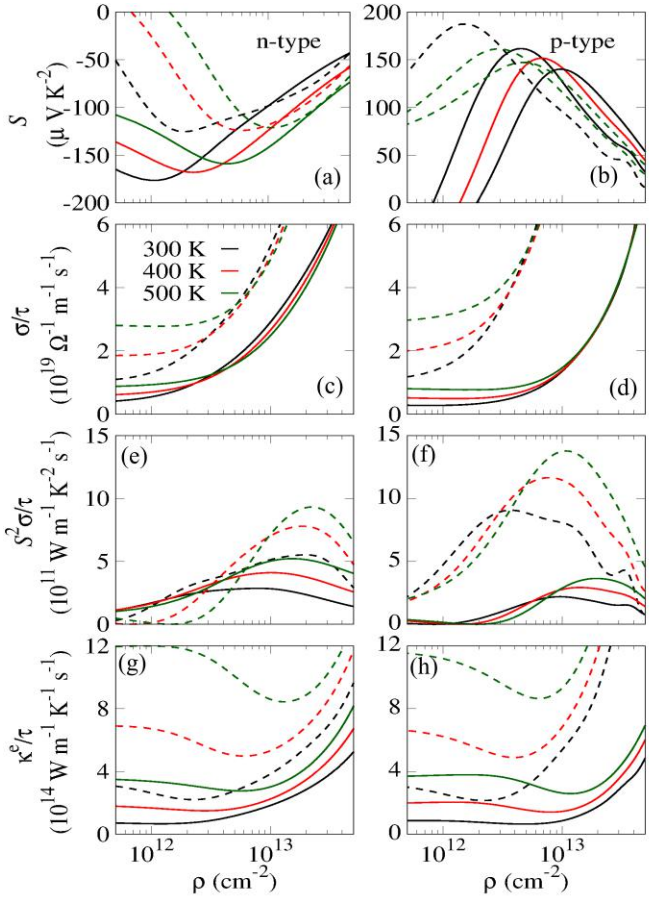

FIG. 6. (a,b) Seebeck coefficient, (c,d) electrical conductivity, (e,f) power factor, (g,h) electronic thermal conductivity as a function of the carrier concentration for both n-type and p-type at 300 K, 400 K, and 500 K of the monolayer C6N. The solid and dashed lines represent the x- and y-direction, respectively.

using the following equations:

$$S^{\alpha\beta}(T,\mu) = \frac{1}{eT\Omega\sigma^{\alpha\beta}(T,\mu)} \int \sigma^{\alpha\beta}(\epsilon)(\epsilon-\mu)\left[-\frac{\partial f_0(T,\epsilon,\mu)}{\partial\epsilon}\right] d\epsilon \tag{4}$$

$$\sigma^{\alpha\beta}(T,\mu) = \frac{1}{\Omega} \int \sigma^{\alpha\beta}(\epsilon)\left[-\frac{\partial f_0(T,\epsilon,\mu)}{\partial\epsilon}\right] d\epsilon \tag{5}$$

$$\kappa_e^{\alpha\beta}(T,\mu) = \frac{1}{e^2T\Omega} \int \sigma^{\alpha\beta}(\epsilon)(\epsilon-\mu)^2\left[-\frac{\partial f_0(T,\epsilon,\mu)}{\partial\epsilon}\right] d\epsilon \tag{6}$$

where T, Ω, μ and $\sigma^{\alpha\beta}(\epsilon)$ represents the temperature, volume of the unit cell, chemical potential and transport distribution function, respectively. The $\sigma_{\alpha\beta}$ can be calculated using the following equation:

$$\sigma_{\alpha\beta}(\epsilon) = e^2 \sum_{\vec{k}} \tau_i(\vec{k}) v_i^{\alpha}(\vec{k}) v_i^{\beta}(\vec{k}) \tag{7}$$

where $\tau_i(\vec{k})$ and $v_i^{\alpha}(\vec{k})$ are the carrier relaxation time, carrier group velocity of α component with wave vector

$\vec{k}$ of the i^{th} band, respectively. The maximum Seebeck coefficients of the C_6N monolayer are: 174 and 188 μV/K for electrons and holes along the x and y directions, respectively. Such large values of the Seebeck coefficient in a semimetal can be related with extra parabolic band in the valence band and a flat conduction band. Secondly, the electrical conductivity (σ/τ) and electronic thermal conductivity (κ^e/τ) are investigated and the results obtained are illustrated in Fig. 6(c-f). The σ/τ and κ^e/τ are increasing with temperature at low carrier concentrations and these quantities become independent at high carrier concentrations. A similar behavior is observed in graphene. The σ/τ and κ^e/τ are greatly larger in the y-direction for n-type and p-type doping. The κ^e/τ is proportional to the σ/τ as demonstrated by the Wiedemann–Franz law: ($\kappa^e = L\sigma T$), where L represents the Lorenz number. The power factor (PF) is also calculated, since it is a very important thermoelectric parameter and it relates the Seebeck coefficient and electrical conductivity by: $PF = S^2\sigma/\kappa^e$. Larger PF values are recored in thermoelectric applications. The Fig. 6(g, h) depicts the PF of the monolayer as function of carrier concentration and temperature. We have obtained considerably larger PF values 13.76, 11.71, and 9.12 (10^{11} $Wm^{-1}K^{-2}s^{-1}$) for the p-type doping at 300 K, 400 K, and 500 K, respectively. These results suggest that the C_6N monolayer is highly promising for thermoelectric application.

VIII. CONCLUSION

In this work, we proved theoretically the dynamical stability of C_6N monolayer by means of first-principles calculations. Dynamical stability of the C_6N monolayer was verified in terms of its phonon band dispersions, while the molecular dynamics simulations revealed the thermal stability. Our results show that the C_6N monolayer has large negative in-plane Poisson's ratios along both X and Y direction. The electronic structure showed that C_6N monolayer is a semi-metal with a Dirac-point. The optical computations indicate that the first and second absorption peaks of this novel 2D structure along in-plane polarization are located in the IR and visible range, respectively. Moreover, the absorption coefficient and optical conductivity of this nanosheet in the UV-vis window. The monolayer of C_6N can be considered for thermoelectric application in which the power factor can reach 13.76, 11 ($10^{11}Wm^{-1}K^{-2}s^{-1}$). Thus, we have demonstrated that the C_6N monolayer can be an alternative C-based 2D material with fascinating properties.

IX. CONFLICTS OF INTEREST

The authors declare that there are no conflicts of interest regarding the publication of this paper.

X. ACKNOWLEDGMENTS

This work was supported by the National Research Foundation of Korea (NRF) grant funded by the Korea government (MSIT) (NRF-2017R1A2B2011989).

* bafekry.asad@gmail.com

[1] K.S. Novoselov, A.K. Geim, S. V. Morozov, D.A. Jiang, Y.Y. Zhang, S. V. Dubonos, A.A. Firsov, I. V. Grigorieva, A.A. Firsov, Sci. 306 (2004) 666-669.
[2] Y. Zhu, S. Murali, W. Cai, X. Li, J.W. Suk, J.R. Potts, R.S. Ruoff, Adv. Mater. 22 (2010) 3906-3924.
[3] A.O.M. Almayyali, B.B. Kadhim, H.R. Jappor, Phys. E Low-Dimensional Syst. Nanostructures 118 (2020) 113866.
[4] A.O.M. Almayyali, B.B. Kadhim, H.R. Jappor, Chem. Phys. 532 (2020) 110679.
[5] A.A. Balandin, S. Ghosh, W. Bao, I. Calizo, D. Teweldebrhan, F. Miao, C.N. Lau, Nano Lett. 8 (2008) 902-907.
[6] W. Cai, Y. Zhu, X. Li, R.D. Piner, R.S. Ruoff, Appl. Phys. Lett. 95 (2009) 123115.
[7] I.W. Frank, D.M. Tanenbaum, A.M. van der Zande, P.L. McEuen, Nanom. Struct. 25 (2007) 2558.
[8] C.D. Reddy, S. Rajendran, K.M. Liew, Nanotechnol. 17 (2006) 864-870.
[9] X. Li, Y. Zhu, W. Cai, M. Borysiak, B. Han, D. Chen, R.D. Piner, L. Colomba, R.S. Ruoff, Nano Lett. 9 (2009) 4359-4363.
[10] S. V. Morozov, K.S. Novoselov, M.I. Katsnelson, F. Schedin, D.C. Elias, J.A. Jaszczak, A.K. Geim, Phys. Rev. Lett. 100 (2008) 016602.
[11] K.I. Bolotin, K.J. Sikes, Z. Jiang, M. Klima, G. Fudenberg, J. Hone, P. Kim, H.L. Stormer, Solid State Commun. 146 (2008) 351-355.
[12] J.W. Jiang, J.S. Wang, B. Li, Phys. Rev. B 80 (2009) 113405.
[13] K.S. Novoselov, Z. Jiang, Y. Zhang, S. V. Morozov, H.L. Stormer, U. Zeitler, J.C. Maan, G.S. Boebinger, P. Kim, A.K. Geim, Sci. 315 (2007) 1379-1379.
[14] S. V. Dubonos, I. V. Grigorieva, K.S. Novoselov, S. V. Morozov, A.A. Firsov, A.K. Geim, M.I. Katsnelson, D. Jiang, S. V. Morozov, D. Jiang, M.I. Katsnelson, I. V. Grigorieva, S. V. Dubonos, A.A. Firsov, Nat. 438 (2005) 197-200.
[15] M. Kim, N.S. Safron, E. Han, M.S. Arnold, P. Gopalan, Nano Lett. 10 (2010) 1125-1131.
[16] W. Liu, L. Zhao, E. Zurek, J. Xia, Y. hao Zheng, H. qing Lin, J. yao Liu, M. sheng Miao, Building egg-tray-shaped graphenes that have superior mechanical strength and band gap, Npj Comput. Mater. 5 (2019) 1-8.
[17] B. Ram, H. Mizuseki, Carbon 158 (2020) 827-835.
[18] W. Choi, N. Choudhary, G.H. Han, J. Park, D. Akinwande, Y.H. Lee, Mater. Today. 20 (2017) 116-130.

[19] J. Bao, M. Edwards, S. Huang, Y. Zhang, Y. Fu, X. Lu, Z. Yuan, K. Jeppson, J. Liu, J. Phys. D. Appl. Phys. 49 (2016) 265501.

[20] M. Zhong, S. Zhang, L. Huang, J. You, Z. Wei, X. Liu, J. Li, Nanoscale 9 (2017) 3736-3741.

[21] A. Lherbier, S.M.-M. Dubois, X. Declerck, Y.-M. Niquet, S. Roche, J.-C. Charlier, Phys. Rev. B. 86 (2012) 075402.

[22] B. Mortazavi, Z. Fan, L.F.C. Pereira, A. Harju, T. Rabczuk, Carbon 103 (2016) 318-326.

[23] C. Metzger, S. Remi, M. Liu, S. V. Kusminskiy, A.H. Castro Neto, A.K. Swan, B.B. Goldberg, Nano Lett. 10 (2010) 6-10.

[24] F. Guinea, M.I. Katsnelson, A.K. Geim, Nat. Phys. 6 (2010) 30-33.

[25] A. Bafekry, and M. Neek-Amal, Phys. Rev. B, 101, 8, (2020), 085417.

[26] A. Bafekry, C. Stampfl Phys. Rev. B 102 (19), (2020) 195411.

[27] A. Bafekry, C. Stampfl, M. Ghergherehchi, Nanotechnol.,31, (2020),295202.

[28] X. Miao, S. Tongay, M.K. Petterson, K. Berke, A.G. Rinzler, B.R. Appleton, A.F. Hebard, Nano Lett. 12 (2012) 2745-2750.

[29] Y.C. Rao, Z.Q. Chu, X. Gu, X.M. Duan, Comput. Mater. Sci. 161 (2019) 53-57.

[30] S. Zhang, J. Zhou, Q. Wang, P. Jena, J. Phys. Chem. C. 120 (2016) 3993-3998.

[31] J. Mahmood, E.K. Lee, M. Jung, D. Shin, I.Y. Jeon, S.M. Jung, H.J. Choi, J.M. Seo, S.Y. Bae, S.D. Sohn, N. Park, J.H. Oh, H.J. Shin, J.B. Baek, Nat. Commun. 6 (2015).

[32] A. Bafekry, M. Yagmurcukardes, M. Shahrokhi, M. Ghergherehchi, Carbon, 168, (2020), 220-229.

[33] A. Bafekry, A. Bafekry, M. Yagmurcukardes, B. Akgenc, M. Ghergherehchi, C. V. Nguyen, J. Phys. D. Appl. Phys. 53 (2020) 355106.

[34] A. Bafekry, S.F. Shayesteh, F.M. Peeters, Phys. Chem. Chem. Phys. 21 (2019) 21070-21083.

[35] A. Bafekry, S.F. Shayesteh, F. Peeters, J. Phys. Chem. C. 123 (2019) 12485-12499.

[36] J. Zeng, Z. Chen, X. Zhao, W. Yu, S. Wu, J. Lu, K.P. Loh, J. Wu, ACS Appl. Nano Mater. 2 (2019) 12.

[37] G.P. Mane, S.N. Talapaneni, K.S. Lakhi, H. Ilbeygi, U. Ravon, K. Al-Bahily, T. Mori, D.H. Park, A. Vinu, Angew. Chemie. 56 (2017) 8481-8485.

[38] P. Kumar, E. Vahidzadeh, U.K. Thakur, P. Kar, K.M. Alam, A. Goswami, N. Mahdi, K. Cui, G.M. Bernard, V.K. Michaelis, K. Shankar, J. Am. Chem. Soc. 141 (2019) 5415-5436.

[39] B. Mortazavi, F. Shojaei, M. Shahrokhi, M. Azizi, T. Rabczuk, A. V. Shapeev, X. Zhuang, Carbon 167 (2020) 40-50.

[40] Q. Xiang, J. Yu, M. Jaroniec, J. Phys. Chem. C 115 (2011) 7355-7363.

[41] A. Bafekry, C. Stampfl, B. Akgenc, M. Ghergherehchi, Phys. Chem. Chem. Phys. 22, 2249-2261

[42] T. Li, C. He, W. Zhang, J. Mater. Chem. A 7 (2019) 4134-4144.

[43] B. Mortazavi, M. Shahrokhi, A. V Shapeev, T. Rabczuk, X. Zhuang, J. Mater. Chem. C 7 (2019) 10908-10917.

[44] F. Li, Y. Qu, M. Zhao, Carbon 95 (2015) 51-57.

[45] A. Bafekry, C. Stampfl, B. Akgenc, B. Mortazavi, M. Ghergherehchi, C. Nguyen Phys. Chem. Chem. Phys. 22 (11), (2020) 6418-6433.

[46] Z. Tian, T. Heil, J. Schmidt, S. Cao, M. Antonietti, ACS Appl. Mater. Interfaces. 12 (2020) 13127-13133.

[47] A. Bafekry,C. V. Nguyen, A. Goudarzi, M. Ghergherehchi andM. Shafieirad, RSC Adv., 10, (2020) 27743-27751.

[48] H. Chen, S. Zhang, W. Jiang, C. Zhang, H. Guo, Z. Liu, Z. Wang, F. Liu, X. Niu, J. Mater. Chem. A 6 (2018) 11252-11259.

[49] H.J. Xiang, B. Huang, Z.Y. Li, S.H. Wei, J.L. Yang, X.G. Gong, Phys. Rev. X 2 (2012) 1-7.

[50] J. Li, C. Cao, J. Hao, H. Qiu, Y. Xu, H. Zhu, Diam. Relat. Mater. 15 (2006) 1593-1600.

[51] A. Thomas, A. Fischer, F. Goettmann, M. Antonietti, J.-O. Muller, R. Schlogl, J.M. Carlsson, J. Mater. Chem. 18 (2008) 4893.

[52] M. Groenewolt, M. Antonietti, Adv. Mater. 17 (2005) 1789-1792.

[53] B. Mortazavi, Carbon 118 (2017) 25-34.

[54] V.N. Khabashesku, J.L. Zimmerman, J.L. Margrave, Chem. Mater. 12 (2000) 3264-3270.

[55] J.S. Lee, X. Wang, H. Luo, S. Dai, Adv. Mater. 22 (2010) 1004-1007.

[56] L.F. Villalobos, M.T. Vahdat, M. Dakhchoune, Z. Nadizadeh, M. Mensi, E. Oveisi, D. Campi, N. Marzari, K.V. Agrawal, Sci. Adv. 6 (2020) eaay9851.

[57] S. Yang, W. Li, C. Ye, G. Wang, H. Tian, C. Zhu, P. He, G. Ding, X. Xie, Y. Liu, Y. Lifshitz, S.T. Lee, Z. Kang, M. Jiang, Adv. Mater. 29 (2017).

[58] Y. Zheng, J. Liu, J. Liang, M. Jaroniec, S.Z. Qiao, Energy Environ. Sci. 5 (2012) 6717-6731.

[59] J. Li, W. Cui, Y. Sun, Y. Chu, W. Cen, F. Dong, J. Mater. Chem. A 5 (2017) 9358-9364.

[60] S.U. Lee, R. V. Belosludov, H. Mizuseki, Y. Kawazoe, Small 5 (2009) 1769-1775.

[61] X.H. Li, X. Wang, M. Antonietti, Chem. Sci. 3 (2012) 2170-2174.

[62] J. Zhang, M. Grzelczak, Y. Hou, K. Maeda, K. Domen, X. Fu, M. Antonietti, X. Wang, Chem. Sci. 3 (2012) 443-446.

[63] J.W. Jiang, X.C. Wang, Y. Song, W.B. Mi, Appl. Surf. Sci. 440 (2018) 42-46.

[64] G.C. Guo, R.Z. Wang, B.M. Ming, C. Wang, S.W. Luo, C. Lai, M. Zhang, Appl. Surf. Sci. 475 (2019) 102-108.

[65] X. Zhao, D. Pan, X. Chen, R. Li, T. Jiang, W. Wang, G. Li, D.Y.C. Leung, Appl. Surf. Sci. 467-468 (2019) 658-665.

[66] B. Mortazavi, M. Shahrokhi, M.E. Madjet, M. Makaremi, S. Ahzi, T. Rabczuk, Carbon 141 (2019) 291-303.

[67] B. Mortazavi, M. Makaremi, M. Shahrokhi, Z. Fan, T. Rabczuk, Carbon 137 (2018) 57-67.

[68] Y. Yong, H. Cui, Q. Zhou, X. Su, Y. Kuang, X. Li, Appl. Surf. Sci. 487 (2019) 488-495.

[69] O. Faye, U. Eduok, J.A. Szpunar, A.C. Beye, Phys. E Low-Dimensional Syst. Nanostructures 117 (2020) 113794.

[70] X. Zhang, A. Chen, Z. Zhang, M. Jiao, Z. Zhou, Nanoscale Adv. 1 (2019) 154-161.

[71] Y. He, M. Zhang, J.J. Shi, Y.H. Zhu, Y.L. Cen, M. Wu, W.H. Guo, Y.M. Ding, J. Phys. D. Appl. Phys. 52 (2019) 015304.

[72] J.N. Grima, S. Winczewski, L. Mizzi, M.C. Grech, R. Cauchi, R. Gatt, D. Attard, K.W. Wojciechowski, J. Rybicki, Adv. Mater. 27 (2015) 1455-1459.

[73] M.T. Lusk, L.D. Carr, Phys. Rev. Lett. 100 (2008) 175503.

[74] J. P. Perdew, K. Burke, M. Ernzerhof, Phys. Rev. Lett. 77 (1996) 3865.

[75] N. Troullier, J. Martins, Phys. Rev. B 43 (1991) 1993.
[76] T. Ozaki, K. Nishio, H. Kino, Phys. Rev. B 81 (2010) 035116.
[77] T. Ozaki, Phys. Rev. B 67 (2003) 155108.
[78] T. Ozaki, H. Kino, Phys. Rev. B 69 (2004) 195113.
[79] Monkhorst, H. J. Pack, J. D. Phys. Rev. B 13 (1976) 5188.
[80] T. Bucko, J. Hafner, S. Lebegue and J. G. Angyan, Phys. Chem. A 114 (2010) 118145.
[81] J. Tersoff and D. R. Hamann. Phys. Rev. Lett. 50 (1983) 1998-2001.
[82] I. Horcas, R. Fernndez, J. M. Gmez-Rodrguez, J. Colchero, J. Gmez-Herrero, and A. M. Baro. Rev. Scient. Inst. 78 (2007) 013705.
[83] M. Gajdos, K. Hummer, G. Kresse, J. Furthmuller, F. Bechstedt, Phys. Rev. B 73, 045112, (2006).
[84] Heyd, J., Scuseria, G. E., J. Chem. Phys. 2004, 121 (3), 1187-1192.
[85] K. Schwarz, P. Blaha, WIEN2k: Comput. Mater. Sci. (2003), 259-273,
[86] B. Mortazavi, I.S. Novikov, E. V Podryabinkin, S. Roche, T. Rabczuk, A. V Shapeev, X. Zhuang, Appl. Mater. Today.20 (2020) 100685.
[87] B. Mortazavi, E. V Podryabinkin, I.S. Novikov, T. Rabczuk, X. Zhuang, A. V Shapeev, Comput. Phys. Commun. 258 (2021) 107583.
[88] B. Mortazavi, E. V Podryabinkin, S. Roche, T. Rabczuk, X. Zhuang, A. V Shapeev, Mater. Horizons. 7 (2020) 2359-2367.
[89] A. V. Shapeev, Multiscale Model. Simul. 14 (2016) 1153-1173.
[90] V. Botu, R. Batra, J. Chapman, R. Ramprasad, J. Phys. Chem. C 121 (2017) 511-522.
[91] I. S. Novikov, K. Gubaev, E. Podryabinkin, A. V. Shapeev, Mach. Learn.: Sci. Technol. (2020).
[92] A. Togo, I. Tanaka, Scr. Mater. 108 (2015) 1-5.
[93] G. K. H. Madsen, J. Carrete, and M. J. Verstraete, Comput. Phys. Commun. 231 (2018) 140-145.
[94] Sh. Zhang, J. Zhou, Q. Wang, and P. Jena, J. Phys. Chem. C 120(7) (2016) 3993-3998.
[95] K. Yin, P. Gao, X. Shao, B. Gao, H. Liu, J. Lv, J. S. Tse, Y. Wang and Y. Ma, npj Comput. Mater. 6 (128) (2020).
[96] B. Wang, Q. Wu, Y. Zhang, L. Ma, and J. Wang, ACS Appl. Mater. Interfaces 11(36) (2019) 33231-33237.
[97] Q. Yue, Sh. Chang, J. Kang, Sh. Qin, and J. Li, J. Phys. Chem. C 117(28) (2013) 14804-14811.
[98] Z. Gao, X. Dong, N. Li, and J. Ren, Nano Lett. 17(2) (2017) 772-777.
[99] Sh. Qian, X. Sheng, Y. Zhou, X. Yan, Y. Chen, Y. Huang, X. Huang, E. Feng, and W. Huang, J. Phys. Chem. C 122(14) (2018) 7959-7967.
[100] M. Li, K. Yuan, Y. Zhao, Zh. Gao, and X. Zhao, ACS Omega 5(2) (2020) 15783-15790.
[101] Sh. Shen, Y. Ma, H. Wang, B. Huang, and Y. Dai, ACS Appl. Mater. Interfaces 35(11) (2019) 31793-31798.
[102] Zhou, Qian Wang, X. Chen, Y. Kawazoe, and P. Jena, PNAS 112(8) (2015) 2372-2377.
[103] F. Wooten, Academic press (2013).
[104] M. Shahrokhi, S. Naderi, A. Fathalian, Solid State Commun., 152 (2012), 1012-1017.
[105] L. Yang, J. Deslippe, C.H. Park, M.L. Cohen, S.G. Louie, Phys. Rev. Lett., 103 (2009), 186802.
[106] M. Shahrokhi, C. Leonard, J. Alloys Compd., 693 (2017), pp. 1185-1196,
[107] Y. Bai, K. Zhou, N. Srikanth, J.H.L. Pang, X. He, R. Wang, RSC Adv., 6 (2016), 35731-35739.
[108] H. Yuan, et al. Nat. Nanotechnol. 10 (2015), 707.

* bafekry.asad@gmail.com